 doi:10.20944/preprints202104.0674.v1

Numerical investigation of the full-scale resistance of a zero-emission fast catamaran in shallow water

Guangyu Shi[1], Alexandros Priftis[1], Yan Xing-Kaeding[2], Evangelos Boulougouris[1,*]
Apostolos D. Papanikolaou[2,3], Haibin Wang[1] and Geoff Symonds[4]

[1]Maritime Safety Research Centre (MSRC), Department of Naval Architecture, Ocean and Marine Engineering, University of Strathclyde, Glasgow, G4 0LZ, United Kingdom.

[2]Computational Fluid Dynamics Department, Hamburg Ship Model Basin (HSVA), Hamburg, Germany.

[3]Ship Design Laboratory, National Technical University of Athens (NTUA), Athens, Greece.

[4]Uber Boat by Thames Clippers, London, United Kingdom.

[*]Email address for correspondence: evangelos.boulougouris @strath.ac.uk.

The present paper investigates numerically the resistance at full-scale of a zero-emission, high-speed catamaran in both deep and shallow water, with the Froude number ranging from 0.2 to 0.8. The numerical methods are validated by two means: a) comparison with available model tests; b) a blind validation using two different flow solvers. The resistance, sinkage and trim of the catamaran, as well as the wave pattern, longitudinal wave cuts and cross-flow fields, are examined. The total resistance curve in deep water shows a continuous increase with the Froude number while in shallow water, a hump is witnessed near the critical speed. This difference is mainly caused by the pressure component of total resistance, which is significantly affected by the interaction between the wave systems created by the demihulls. The pressure resistance in deep water is maximised at a Froude number around 0.58, whereas the peak in shallow water is achieved near the critical speed (Froude number ≈ 0.3). Insight into the underlying physics is obtained by analysing the wave creation between the demihulls. Profoundly different wave patterns within the inner region are observed in deep and shallow water. Specifically, in deep water, both crests and troughs are generated and moved astern as the increase of the Froude number. The maximum pressure resistance is accomplished when the secondary trough is created at the stern, leading to the largest trim angle. In contrast, the catamaran generates a critical wave normal to the advance direction in shallow water, which

 doi:10.20944/preprints202104.0674.v1

significantly elevates the bow and creates the highest trim angle as well as pressure resistance. Moreover, significant wave elevations are observed between the demihulls at supercritical speeds in shallow water which may affect the decision for the location of the wet deck.

Keywords: fast catamaran; shallow water resistance; full-scale CFD

 doi:10.20944/preprints202104.0674.v1

1 Introduction

Low-carbon, environmentally-friendly maritime transport is playing an important role in reducing the emission of greenhouse gases and building a sustainable future. The need for technological innovations in the design of zero-emission ships is posing challenges for the maritime industry in the coming decades. The research presented herein was conducted in the European Commission (EC) funded research project TrAM (Transport: Advanced and Modular, https://tramproject.eu/), which aims at designing and manufacturing battery-powered fast catamarans operating in coastal areas and inland waterways by implementing modular design and production methods. Given the significant lower specific energy content of batteries compared to conventional fuels [1], the design of zero-emission high-speed marine vehicles poses unique challenges and limitations which are tackled within the TrAM project. These include the selection of the appropriate battery technology and specification, safety considerations and of course, multi-objective hull form optimisation in the presence of shallow water effects [1–4]. The present study is focused on the battery-driven, zero-emission 'TrAM London Demonstrator', designed for The Thames River. It examines the hydrodynamic performance of the preliminary design of this high-speed catamaran in shallow water as it affects directly the rate by which the vessel consumes the stored energy. Therefore, it verifies and validates the computational methods employed in the hydrodynamic optimisation of the hull form.

Catamarans, due to their favourable performance in efficiency and stability at high speeds, have been widely studied experimentally, theoretically and numerically over the past decades [5–7]. A series of model tests were carried out by Insel and Molland [8] and Molland et al. [9] investigating the calm water resistance of fast catamarans with symmetrical demihulls, whereas Zaraphonitis et al. [10] have studied asymmetrical demihulls. Their studies emphasised the effects of demihull dimensions and separation distance on the resistances and motions of the catamarans over a wide range of Froude numbers ($0.2 \leq Fn \leq 1.0$). van't Veer [11] also experimentally investigated the resistance and dynamic motion characteristics using Delft 372 catamaran, which has been used as a benchmark for numerical simulations. Later experimental studies with Delft 372 catamaran were concentrated on the hydrodynamic interference between demihulls [12,13] and seakeeping [14–16]. Broglia et al. [13] carried out experimental work examining the interference effects between the demihulls of a catamaran. It was found that positive inference only occurred within a narrow range of testing conditions and the interaction between demihulls

Preprints (www.preprints.org) | NOT PEER-REVIEWED | Posted: 26 April 2021 doi:10.20944/preprints202104.0674.v1

could increase the total resistance by up to 30%. The interference effects were less strong at very low and very high Froude numbers (Fn < 0.3 or Fn > 0.7). Zaraphonitis et.al. [17] studied the optimisation of the hull shape with regards to powering and wash for a high speed catamaran. Souto-Iglesias et al. [18] also investigated experimentally the interference phenomenon of a catamaran and compared the wave systems created by the catamaran and the corresponding monohull. They concluded that the non-centred inner wave cuts are also important evidence for the analysis of wave interference. Later, Souto-Iglesias et al. [19] further studied the influence of demihull separation and testing condition on the interference resistance of a Series 60 catamaran and found that the free sinkage-trim condition enhanced both the favourable and unfavourable interference effects compared with fixed condition cases. Danışman [20] found that the wave interference resistance between the demihulls could be considerably reduced by placing an optimised Centrebulb, which led to a favourable secondary wave interaction.

With the fast development of computer science and numerical methods, computational fluid dynamics (CFD) has become a feasible approach with sufficient accuracy to investigate ship hydrodynamics [21]. Various CFD solvers have been applied to examine the calm water resistance and seakeeping of both monohulls [22–24] and multihulls [25–29]. A combined experimental and numerical study was carried out by Zaghi et al. [30] to analyse the interference effects between the demihulls and the dependency on the separation of a high-speed catamaran. Two humps were found in the total resistance coefficient curves and the second one was much higher, corresponding to a stronger interference. Besides, a smaller separation distance led to a stronger interaction and a larger speed where the peak occurred. Broglia et al. [31] conducted a numerical analysis on the interference phenomena between the demihulls of the catamaran with emphasis on the validation of the CFD code and the Reynolds number effect. It was found that the numerical results agreed very well with the experiment in terms of resistance and wave cuts and the dependency on the scale effect was rather weak. He et al. [32] computationally investigated the effects of Froude number and demihull separation distance on the resistance and motion of the catamaran. They found that the resistance coefficient became higher at smaller separation distances, indicating stronger interference between the demihulls. Besides, the strongest demihull interaction occurred when Froude number is between 0.45 and 0.65 (0.45 < Fn < 0.65). When the Froude number is below 0.45 or above 0.65, the variation of the separation distance had a negligible effect on the resistance as well as the sinkage and trim of the catamaran. Haase et al. [33] proposed a novel CFD-based method for the prediction of full-scale ship resistance, which relied on the results of the model test experiment and CFD simulation at

Preprints (www.preprints.org) | NOT PEER-REVIEWED | Posted: 26 April 2021 doi:10.20944/preprints202104.0674.v1

both model-scale and full-scale Reynold number. Farkas et al. [34] carried out a numerical study on the interference of resistance components for a Series 60 catamaran at medium Froude numbers, where the interference factor was decomposed into viscous interference and wave interference. They found that the form factor of the catamaran was independent of the Froude number, but decreased to the value of the monohull when the separation distance became larger. It was also observed that the viscous interference factor was independent of the Froude number but relied on the separation ratio of the catamaran.

The shallow water effects must be considered when designing ships for restricted waterways (e.g., inland rivers, canals). Previous studies regarding shallow water effects for monohulls [35–39] revealed that the depth Froude number ($Fn_H = U/\sqrt{gH}$, where U is the ship speed, g is gravity acceleration and $H$is the water depth) is playing a key role in determining the performance of the vessel. A ship moving near the critical depth Froude number (Fn_H = 1.0) will experience a surge in total resistance coefficient and drastic changes in motions and wave patterns, which should be taken into account when passing through shallow water areas. In terms of catamarans operating in shallow water, several experimental and numerical studies are also available [40–43]. Molland et al. [44,45] experimentally investigated the resistance of a series of fast displacement catamarans in shallow water. Similar to monohulls, the catamarans experienced large increases in total resistance and wave elevation, and significant changes in sinkage and trim near the critical depth Froude number. The resistance increase was higher for the smaller water depth. Gourlay [46] theoretically predicted the sinkage and trim of various catamaran configurations in shallow water. It was found that the maximum sinkage and trim occurred at the trans-critical speed range. Lee et al. [47] designed and tested the shallow water behaviours of a small catamaran and further investigated the influence of the separation ratio between the demihulls on the resistance characteristics. The residual resistance coefficient surged near the critical depth Froude number and the sinkage and trim also varied significantly in the critical region. Castiglione et al. [48] studied the interference effects between the demihulls of a high-speed catamaran in shallow water using a CFD method. They concluded that for all separation ratios, the total resistance coefficients were significantly increased due to shallow water effects, with peaks achieved near the critical depth Froude number. However, at extreme subcritical and supercritical speeds, the total resistance coefficients in shallow water became smaller than the values of corresponding deepwater cases. It was also found that the interference factor reached its peak values around the critical speed and increased for smaller separation distances. Moreover, the sinkage and trim were also increased compared with deep water values and maximised at the critical speed.

Preprints (www.preprints.org) | NOT PEER-REVIEWED | Posted: 26 April 2021 doi:10.20944/preprints202104.0674.v1

Despite the extensive studies on the calm water resistance and interference of high-speed catamarans, CFD simulations on full-scale fast catamarans in shallow water are still rare. As aforementioned, the work in the present paper is part of the ongoing TrAM Project (https://tramproject.eu/) and the objectives of the current study are twofold: 1) validate the numerical methods and setups that will be employed in the hull optimisation stage, 2) investigate the shallow water effect on the calm water resistance, sinkage, trim and wave creation of the full-scale London Demonstrator catamaran using a CFD method. The rest of this paper is organized as follows: In Section 2, the geometry of the London Demonstrator and parameters used for analysis are presented. The computational methods are introduced in Section 3 and they are validated in Section 3.4. In the next section, the numerical results are given. The conclusions are drawn in the final section.

2 Geometry and Parameters

2.1 Catamaran geometry and dimensions

The London Demonstrator catamaran investigated in the present work is designed by the Maritime Safety Research Centre (MSRC) at the University of Strathclyde, which is a partner at the ongoing EU funded project TrAM (https://tramproject.eu/). The London Demonstrator is designed for The Thames River as a battery-driven, zero-emission passenger ferry. As the catamaran is still at the initial design stage, the geometry illustrated in Figure 1 is selected as a showcase validating the numerical methods and examining the shallow water effect. Some main dimensions of the London Demonstrator are summarised in Table 1, where L_{pp} is the length between perpendiculars.

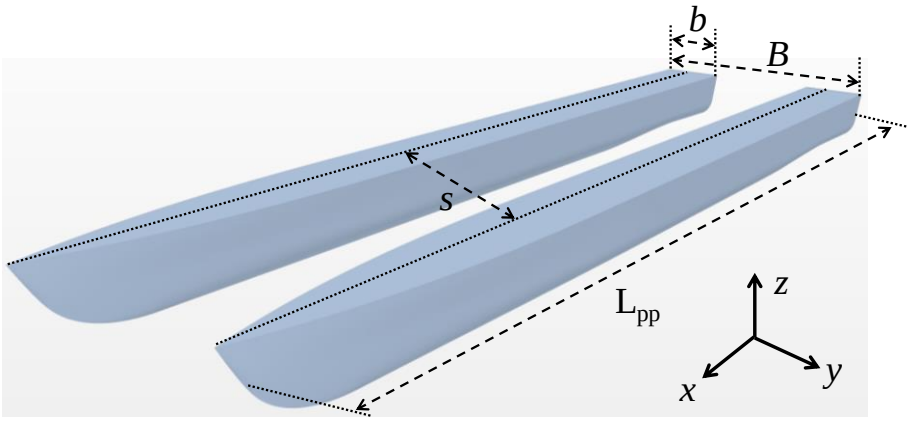

Figure 1 Geometry of London demonstrator.

Preprints (www.preprints.org) | NOT PEER-REVIEWED | Posted: 26 April 2021 doi:10.20944/preprints202104.0674.v1

Table 1 Main dimensions of the TrAM London Demonstrator catamaran.

Dimension	*Symbol*	*Value*[*]
Overall breadth	B/L_{pp}	0.255
Demihull breadth	b/L_{pp}	0.068
Separation	s/L_{pp}	0.187
Draught	T/L_{pp}	0.033
Water depth	H/T	2.0

[*]All values are dimensionless

2.2 Parameters for analysis

In ship hydrodynamics, Froude number is an important non-dimensional parameter measuring the speed of the vessel, which is defined as:

$$Fn = \frac{U}{\sqrt{gL_{pp}}} \tag{1}$$

where U is the ship speed, g is gravity acceleration. For ships advancing in shallow waterways, the Froude number defined based on the water depth is playing a significant role in determining the ship hydrodynamics:

$$Fn_H = \frac{U}{\sqrt{gH}} \tag{2}$$

The hydrodynamic performance of the TrAM London Demonstrator is analysed by examining its total resistance (R_T), sinkage (σ) and trim (θ). The total resistance is decomposed into the frictional component (R_F) and pressure component (R_P), i.e., $R_T = R_F + R_P$. The sinkage and trim are measured based on the centre of mass of the catamaran and they defined as positive when the catamaran goes down and the bow moves up respectively. Moreover, the resistance coefficients are also used for analysis. The total resistance coefficient is defined as

$$C_T = \frac{R_T}{0.5\rho U^2 S} \tag{3}$$

Similarly, the frictional and pressure resistance coefficients can be formulated as

Preprints (www.preprints.org) | NOT PEER-REVIEWED | Posted: 26 April 2021 doi:10.20944/preprints202104.0674.v1

$$C_F = \frac{R_F}{0.5\rho U^2 S}$$
$$C_P = \frac{R_P}{0.5\rho U^2 S} \quad (4)$$

where ρ is the water density, U is the moving speed of the catamaran and $S \in (S_{sw}, S_{dw})$ is the wetted surface area, where S_{sw} and S_{dw} are the static and dynamic wetted surface areas respectively. The frictional resistance coefficient can also be estimated by the ITTC 1957 correlation line formula

$$C_{T,ITTC} = \frac{0.075}{[log_{10}(Re) - 2]^2} \quad (5)$$

3 Methodology

3.1 Computational methods

3.1.1 Flow simulation

The unsteady incompressible turbulent flow in the present study is simulated by solving the unsteady Reynolds-Averaged Navier-Stokes (URANS) equations. The corresponding continuity and momentum equations can be formulated as

$$\frac{\partial \overline{u_\iota}}{\partial x_i} = 0 \quad (6)$$

$$\frac{\partial \overline{u_\iota}}{\partial t} + \frac{\partial}{\partial x_j}\left(\overline{u_\iota}\,\overline{u_\jmath} + \overline{u_\iota' u_\jmath'}\right) + \frac{1}{\rho}\frac{\partial \bar{p}}{\partial x_i} - \frac{\partial \overline{\tau_{\iota\jmath}}}{\partial x_j} = 0 \quad (7)$$

where ρ is the fluid density, x_i and x_i are the components of the position vector in Cartesian coordinate, $\overline{u_\iota}$ and $\overline{u_\jmath}$ are the components of the mean velocity vector, $\overline{u_\iota' u_\jmath'}$ is the Reynolds stresses and $\bar{p}$ is the mean pressure. $\overline{\tau_{\iota\jmath}}$ are the components of the mean viscous stress tensor, which can be written as

$$\overline{\tau_{\iota\jmath}} = \nu\left(\frac{\partial \overline{u_\iota}}{\partial x_j} + \frac{\partial \overline{u_\jmath}}{\partial x_i}\right) \quad (8)$$

where ν is the fluid kinematic viscosity.

The $k-\omega$ SST turbulence model, which has been widely used for marine hydrodynamics [21,29,32], is employed as the closure for Eq. (6) and (7). Here, the flow governing equations including the turbulent model are solved using a finite volume method implemented in the commercial code Star CCM+ 14.06.

Preprints (www.preprints.org) | NOT PEER-REVIEWED | Posted: 26 April 2021 doi:10.20944/preprints202104.0674.v1

The Semi-Implicit Method for Pressure-Linked Equations (SIMPLE) was used as the solution procedure, where the continuity and momentum equations are solved sequentially and then coupled via a predictor-corrector approach. The spatial discretisation was achieved using a second-order scheme while a first-order scheme was employed for temporal discretisation since we are only focused on the final converged equilibrium state.

3.1.2 Free surface capturing

For marine hydrodynamics, the appropriate capture of the free surface is of great importance in order to accurately predict the wave height. In the present work, the volume of fluid (VOF) method in combination with the High-Resolution Interface Capturing (HRIC) scheme was adopted to calculate the wave elevation induced by the motion of the catamaran. To avoid the wave's reflection at the boundaries of the computational domain, a wave forcing method was used at relevant boundaries to guarantee that the wave is completely damped out when it reaches the domain boundary. The wave forcing length and relevant boundaries are illustrated in Figure 3.

3.1.3 Dynamic trim and sinkage

As the catamaran is advancing in the water, the surface of the hull will interact with the surrounding water, leading to a fluid-body interaction problem. In the present study, only the heave and pitch motions were allowed while the rest degrees of freedom were fixed. The Dynamic Fluid-Body Interaction (DFBI) method provided in Star CCM+ 14.06 package was employed to calculate the sinkage and trim of the catamaran according to the fluid forces and moments acting on the hull surface. As the overset grid strategy was used in the present study, the DFBI method was only applied to the demi-hull and its associated region (see section 3.2).

3.1.4 Coordinate system

In the present simulation, two different coordinate systems are used: an earth-fixed (global) system and a ship-fixed (local) system. The flow simulation was carried out within the earth-fixed coordinate system and the computed forces and moments were then transformed to the ship-fixed coordinate system whose origin was located at the centre of mass of the catamaran. The equations of the motion were solved based on the latest forces and moments using the DFBI method. The new position and velocity of the hull were then converted back to the earth-fixed system as the boundary condition for the flow simulation. After

Preprints (www.preprints.org) | NOT PEER-REVIEWED | Posted: 26 April 2021 doi:10.20944/preprints202104.0674.v1

updating the position of the hull, the connectivity between the two sub-domains in the overset grid method was re-calculated accordingly.

3.2 Computational domain and boundary conditions

As the catamaran is geometrically symmetrical about its mid-plane, only one demi-hull was used for CFD simulation in order to reduce computational cost. Besides, the overset grid method was employed in the present study, i.e., the entire computational domain was decomposed into two regions: an inner region around the demi-hull (Hull Region) and an outer region forming the virtual tank (Tank Region). Figure 2 shows the two regions and corresponding boundary conditions. The flow variables between the two flow regions were exchanged at the overlapping boundary via linear interpolation. For deep water scenarios, as demonstrated in Figure 3 (a-b), the Tank Region was extended $1.5L_{pp}$ in front of the hull and $5L_{pp}$ behind it. The lower and upper boundaries were $2.5L_{pp}$ and $1.5L_{pp}$ away from the undisturbed water level respectively. The side boundary of the Tank Region was $2.5L_{pp}$ away from the symmetry plane of the catamaran. The velocity inlet condition was applied at the inlet, top, bottom and side boundaries. The pressure outlet condition was used for the outlet boundary. The demi-hull surface was considered as the no-slip wall. To avoid wave refection, a wave forcing method was applied to the regions near the inlet, outlet and side boundaries, as shown in Figure 3 (a-b). For shallow water scenarios, the size of the Tank Region remained the same as the one used for deep water cases except that the bottom surface was 2.15 metres below the water level (water depth = 2.15 m), where the slip wall boundary condition was applied.

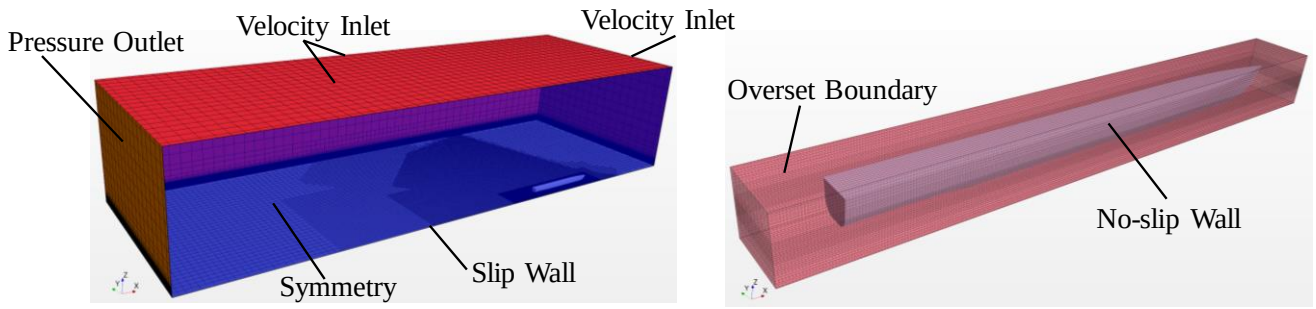

Figure 2 Computational domains (left: Tank Region; right: Hull Region) and boundary conditions.

3.3 Mesh generation

The CFD mesh used in the present study was generated using the automated meshing functionality in Star

Preprints (www.preprints.org) | NOT PEER-REVIEWED | Posted: 26 April 2021 doi:10.20944/preprints202104.0674.v1

CCM+ 14.06, which was comprised of prism cells around the hull and the hexahedral cells in the rest region. The meshes for the Tank Region and Hull Region were generated separately and an overset grid interface was created between the two regions. Anisotropic mesh refinements were performed in various areas in order to appropriately capture the flow features. Specifically, three volumetric mesh controls in three different levels were created around the hull. Similarly, such volumetric mesh controls were also generated to capture the Kelvin waves, the flow wakes behind the hull and the free surface, as demonstrated in Figure 3. All mesh refinements were done by setting a target mesh size relative to a base size specified by the user in the automated meshing tool of Star CCM+ 14.06. The mesh density can also be controlled by varying the value of this base size. Additionally, special attention was given to the overlapping area of the Tank Region and Hull Region when generating the volume mesh. First, the mesh cells within the overlapping region were of similar size. Besides, the overlapping zone was comprised of at least five cell layers in both regions to ensure an accurate and conservative interpolation.

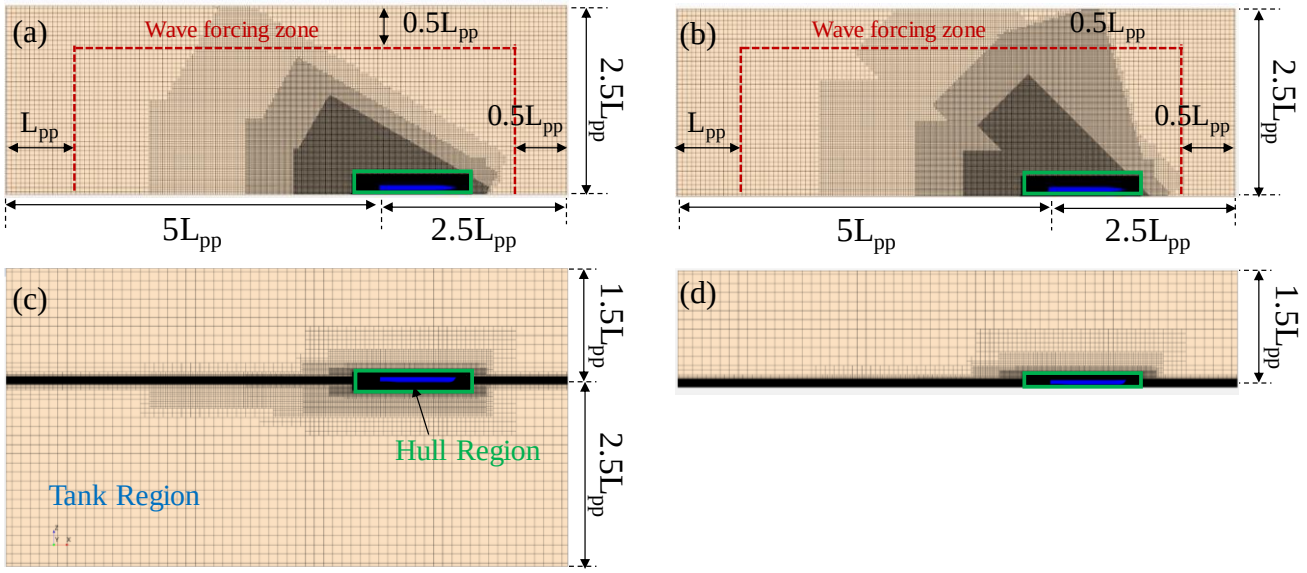

Figure 3 Computational meshes and domain dimensions used for deep water (a, c) and shallow water cases (b, d).

To properly resolve the flow boundary layer, prism mesh layers should be used in the vicinity of the hull. Here, the thickness of the turbulent boundary layer was estimated by

$$\delta = 0.37 L_{pp} / Re^{0.2} \tag{9}$$

where Re is the Reynolds number based on L_{pp}. Ten layers of prism cells were placed within the boundary

Preprints (www.preprints.org) | NOT PEER-REVIEWED | Posted: 26 April 2021 doi:10.20944/preprints202104.0674.v1

layer. As the wall function was used in the turbulent model, the distance of the first prism layer to the hull surface was targeted at y+ =100. Figure 4 demonstrates the computed y+ distribution on the hull surface and it can be observed that for both Froude numbers the y+ values are within the range (30 < y+ < 300) that the wall function can be appropriately applied.

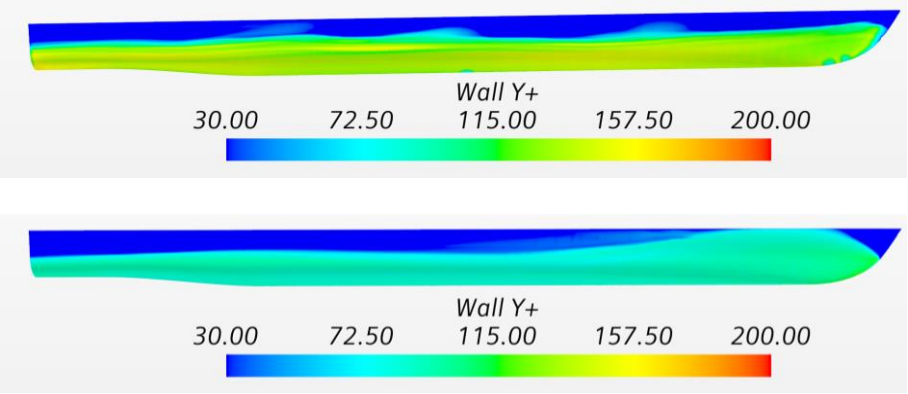

Figure 4 Computed y+ distribution on the demihull surface at Fn = 0.287 (upper) and 0.805 (below) in shallow water.

3.4 Numerical validation

3.4.1 NPL 4a02 catamaran

The first case used to validate the computational methods used in the present study was the NPL 4a02 catamaran from a series of model tests carried out by Molland et al. [9]. The same computational methods and mesh generation strategies presented in Section 3 were also applied here. The total number of mesh cells used for this validation case was around 4.7 million. Figure 5 demonstrates the total resistance coefficients, sinkage-to-draught ratios and trim angles as functions of the Froude number, from which it is observed that the computed results are in good agreement with the experimental data.

Preprints (www.preprints.org) | NOT PEER-REVIEWED | Posted: 26 April 2021 doi:10.20944/preprints202104.0674.v1

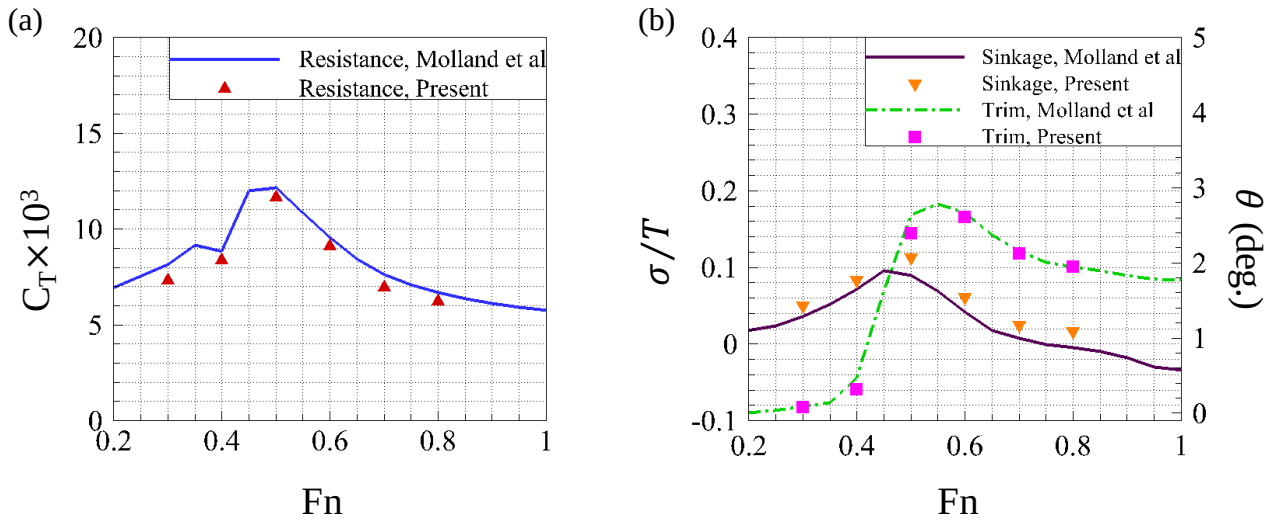

Figure 5 Total resistance coefficients (a), sinkage and trim (b) of NPL 4a02 model.

3.4.2 Stavanger demonstrator

The computational methods presented in Section 3 were further validated against the experimental data of the Stavanger demonstrator [2,3] measured in the Hamburg Ship Model Basin (HSVA). The geometry of the Stavanger demonstrator is illustrated in Figure 6 (a) and the mesh used for simulation is demonstrated in Figure 6 (b), which was consisted of about 11.4 million cells. The computational domain, boundary conditions and mesh system were generated in similar manners to those presented in Section 3. Table 2 compares the total resistance coefficients of the Stavanger demonstrator obtained from CFD simulations with that from physical model tests. It is seen that for the four speeds considered here, the difference between the present numerical result and the experimental data is within 1.5%.

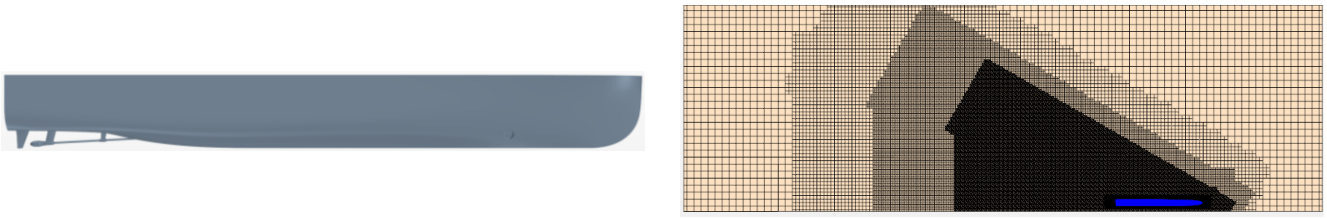

Figure 6 Geometry of Stavanger demonstrator (a) and CFD mesh used for simulation (b).

Preprints (www.preprints.org) | NOT PEER-REVIEWED | Posted: 26 April 2021 doi:10.20944/preprints202104.0674.v1

Table 2 Total resistance coefficient of Stavanger demonstrator obtained from model tests and CFD simulation.

Fn	$C_{T,CFD} \times 10^3$	$C_{T,Exp} \times 10^3$	$Error$
0.57	5.476	5.520	-0.79%
0.63	4.844	4.899	-1.11%
0.69	4.404	4.437	-0.74%
0.75	4.098	4.157	-1.42%

4 Results and Discussion

4.1 Resistance, sinkage and trim

As the present paper aims to validate the numerical methods adopted for simulation, a blind validation study was carried out by MSRC and HSVA, where the commercial solver Star CCM+ 14.06 was used by MSRC whereas an in-house code FreSCo+ [49] was employed by HSVA. The number of mesh cells for both simulations was approximately 6 million. Figure 7 shows the resistances and motions of the full-scale London Demonstrator in deep water, from which we can observe that very good agreement is accomplished between the present results (Strath) and those from HSVA. It is seen from Figure 7 (a) that the total resistance (R_T) rises monotonously as the speed of the catamaran increases. The relation between R_T and Fn is almost linear when $Fn < 0.4$. A continuous change in the slope of the total resistance curve can be observed when $0.4 < Fn < 0.6$, which is also reported by Zaghi et al. [30] in the same Froude number range and indicates the experience of unfavourable interferences. The frictional component (R_F) also rises monotonously with the increase of the speed while the pressure component (R_P) experiences a peak at $Fn = 0.575$. Besides, R_P is the larger component at lower speeds whilst it becomes smaller when Fn is greater than 0.65.

The sinkage and trim are demonstrated in Figure 7 (b) and it is observed that the trim angle of the catamaran is always positive, i.e., the stern goes down for all speeds considered here. At lower speeds ($Fn < 0.4$), the trim angle of the London Demonstrator remains almost zero. When Fn becomes higher than 0.4, it rises significantly and reaches its peak at $Fn = 0.575$ where R_P also achieves its maximum value. In terms of the sinkage of the catamaran, it keeps positive (the hull moves downwards) until the Fn is higher than 0.7. The largest sinkage is experienced at $Fn = 0.517$, which is slightly smaller than the Froude number where the trim maximum is accomplished. It should also be noted that the significant changes in

Preprints (www.preprints.org) | NOT PEER-REVIEWED | Posted: 26 April 2021 doi:10.20944/preprints202104.0674.v1

trim and sinkage occur when $0.4 < Fn < 0.6$, corresponding to the range where the total resistance curve varies. It will be shown in the following sections that these behaviours of resistance and motion are closely associated with the position and strength of the crests and troughs at the central plane of the catamaran.

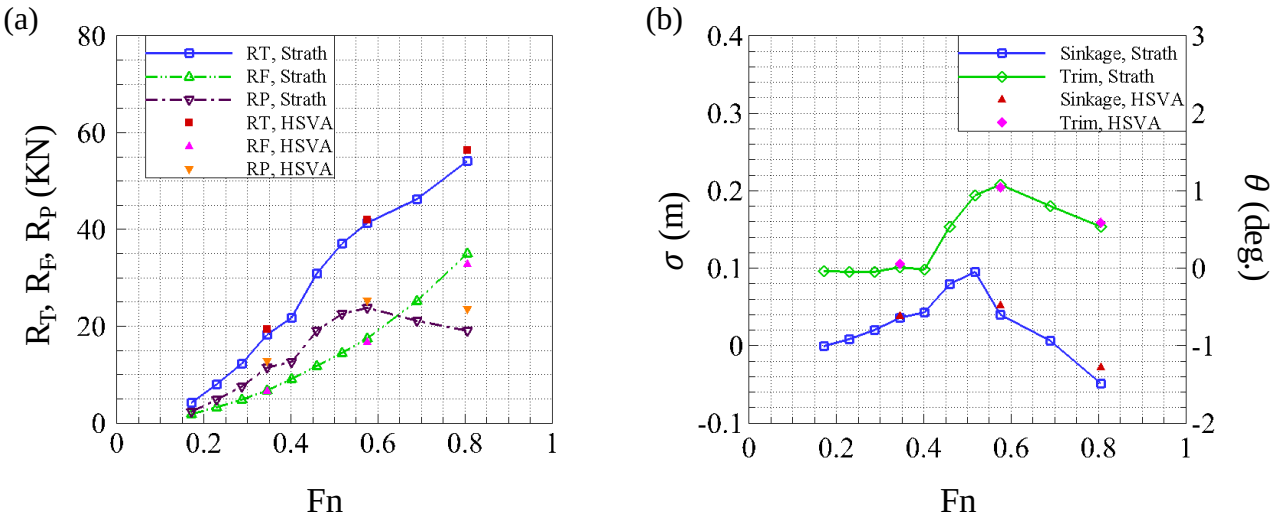

Figure 7 Resistances (a) and motions (b) of the London Demonstrator in deep water.

Figure 8 compares the resistances and motions of the London Demonstrator in shallow water obtained from the present calculation with those computed by HSVA using FreSCo+. It can be seen that the results from both solvers also agree very well with each other for shallow water scenarios. It is interesting to observe from Figure 8 (a) that R_T experiences a hump at $Fn = 0.287$, corresponding to a depth Froude number ($Fn_H = 1.12$) around the critical value. It has been widely acknowledged that fast catamarans will experience a dramatic surge in total resistance coefficient near the critical speed in shallow water [45,48]. However, the existence of such a hump in total resistance rather than the coefficient near the critical depth Froude number is rarely reported in previous studies. R_T rises monotonously after the hump (when $Fn > 0.35$) as the continuous increase of the frictional resistance. An inspection of R_P and R_F curves reveal that the hump comes from the pressure component of the resistance, indicating it is the consequence of wave interference between the demihulls. Different from the total resistance, R_P declines after the hump and the frictional resistance exceeds R_P and becomes the larger part of the total resistance when $Fn > 0.55$. The existence of such a hump in the R_T curve should be carefully considered in the design of the catamaran to guarantee that the installed power is sufficient to overcome the hump resistance in the process of accelerating the vessel to the designed speed. It is observed from Figure 8 (b) that the sinkage and motion of the catamaran change significantly near the critical speed, which agrees with previous studies on high

Preprints (www.preprints.org) | NOT PEER-REVIEWED | Posted: 26 April 2021 doi:10.20944/preprints202104.0674.v1

speed catamarans [45,48].

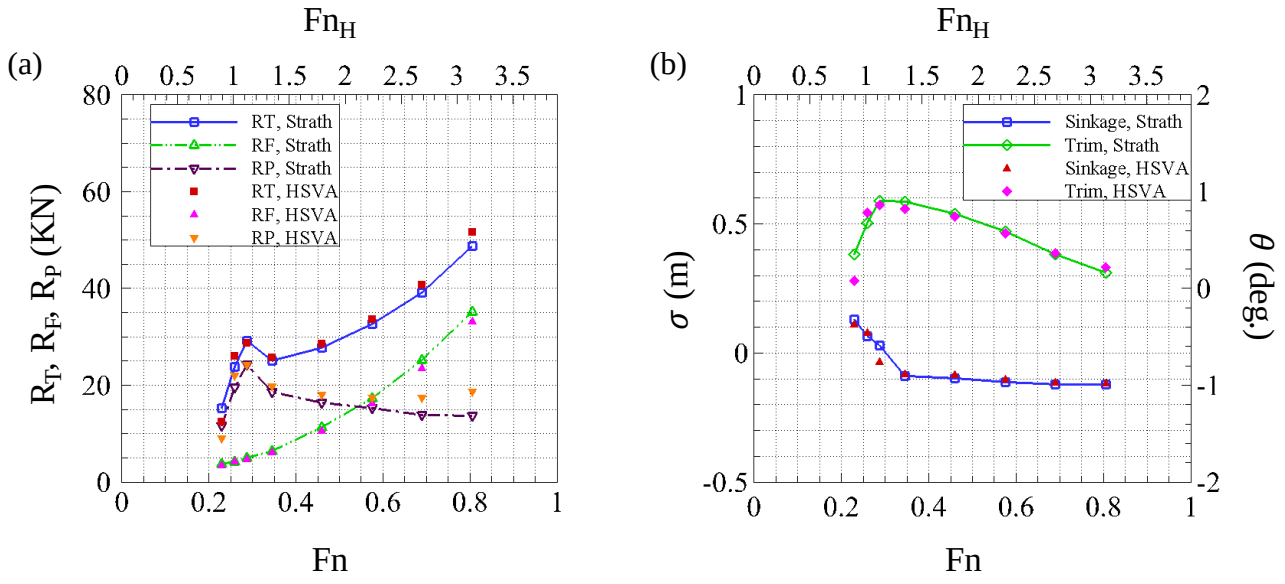

Figure 8 Resistances (a) and motions (b) of the London Demonstrator in shallow water (H = 2.15 m).

Figure 9 compares the resistances and motions of the London Demonstrator in deep and shallow water. Hereafter, only the results computed using Star CCM+ 14.06 are used for further analysis. The total resistance in shallow water is higher than that in deep water at smaller Froude numbers ($Fn < 0.45$) because of the hump near the critical speed. When Fn further increases, R_T in shallow water becomes lower due to the reduction of pressure resistance R_P. The frictional resistances in deep and shallow water are almost the same, i.e., the difference between the total resistance in deep and shallow water results from significantly different wave patterns and interferences, which will be demonstrated in the following sections. By comparing the motions of deep and shallow water cases, it is found that the maximum trim angles accomplished in deep and shallow water are close to each other (≈ 1.0 degree). However, the maximum of trim in shallow water is reached near the critical speed ($Fn = 0.287$) whereas the peak in deep water is achieved at $Fn = 0.575$. Similar to deep water cases, the maximum value of shallow water trim is also achieved at the Froude number where the pressure resistance peaks ($Fn = 0.287$). The sinkage of the catamaran in shallow water is larger in sub- and trans-critical ranges ($Fn < 0.3$) whilst in supercritical region, the sinkage in shallow water becomes smaller than that in deep water, which leads to a considerable reduction in pressure drag, as observed from Figure 9 (a). Furthermore, the sinkage of the catamaran in shallow water is positive at subcritical speeds. With the further increase of Froude number,

Preprints (www.preprints.org) | NOT PEER-REVIEWED | Posted: 26 April 2021 doi:10.20944/preprints202104.0674.v1

the catamaran's centre of mass starts to move upward and when $Fn > 0.35$, the change rate of sinkage becomes less significant.

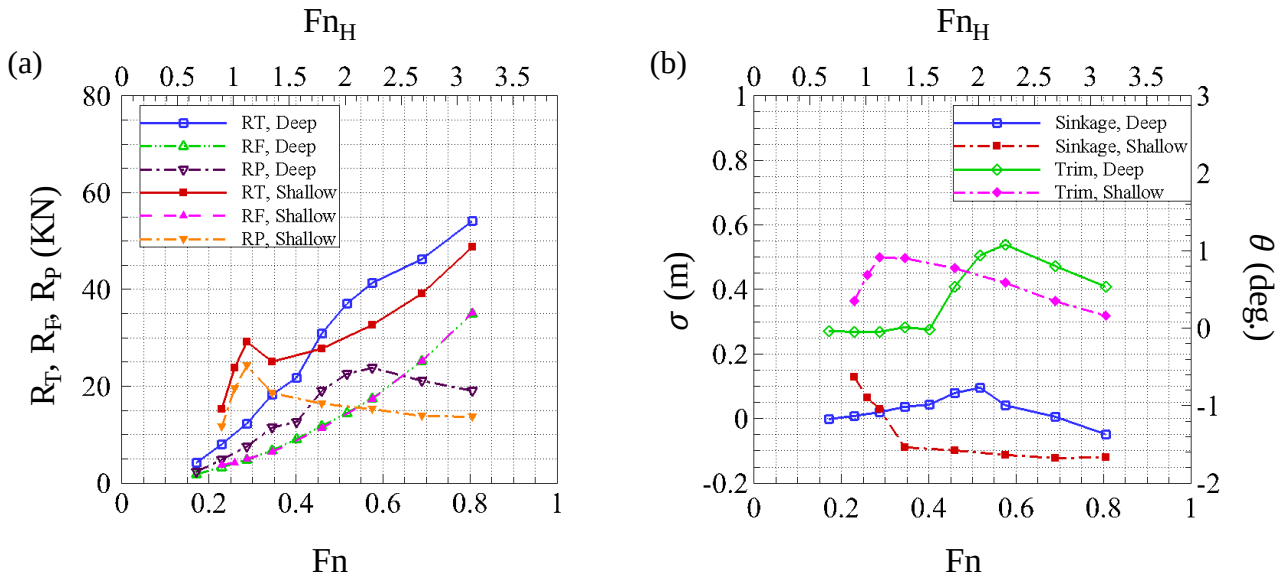

Figure 9 Comparison of resistances (a) and motions (b) of London Demonstrator in deep and shallow water (H = 2.15 m).

The resistance coefficients of the London Demonstrator in deep and shallow water are illustrated in Figure 10 and Figure 11 respectively. The total resistance coefficients (C_T) are normalised using both static and dynamic areas and the differences are small for both deep and shallow water cases. Generally, the coefficients calculated based on the dynamic wetted area are slightly smaller and the difference only becomes noticeable for the highest speed ($Fn \approx 0.8$). The frictional resistance coefficients (C_F) of the catamaran in both deep and shallow water agree well with those predicted using the ITTC 1957 correlation line formula, indicating the frictional resistance is not significantly affected by shallow water. Moreover, for deep water cases shown in Figure 10, C_T and C_P experience multiple peaks as the increase of Froude number. The peaks at lower Froude numbers ($Fn < 0.4$) are higher than that at $Fn = 0.46$. The total resistance coefficient drops significantly as the further increase of the advance speed. The present C_T curve differs from those observed in some previous studies, where the humps at smaller Froude numbers were usually lower [9,13,30]. This may be associated with the exact hull form and configuration of the catamaran, which leads to a different wave interference between the demihulls.

Preprints (www.preprints.org) | NOT PEER-REVIEWED | Posted: 26 April 2021 doi:10.20944/preprints202104.0674.v1

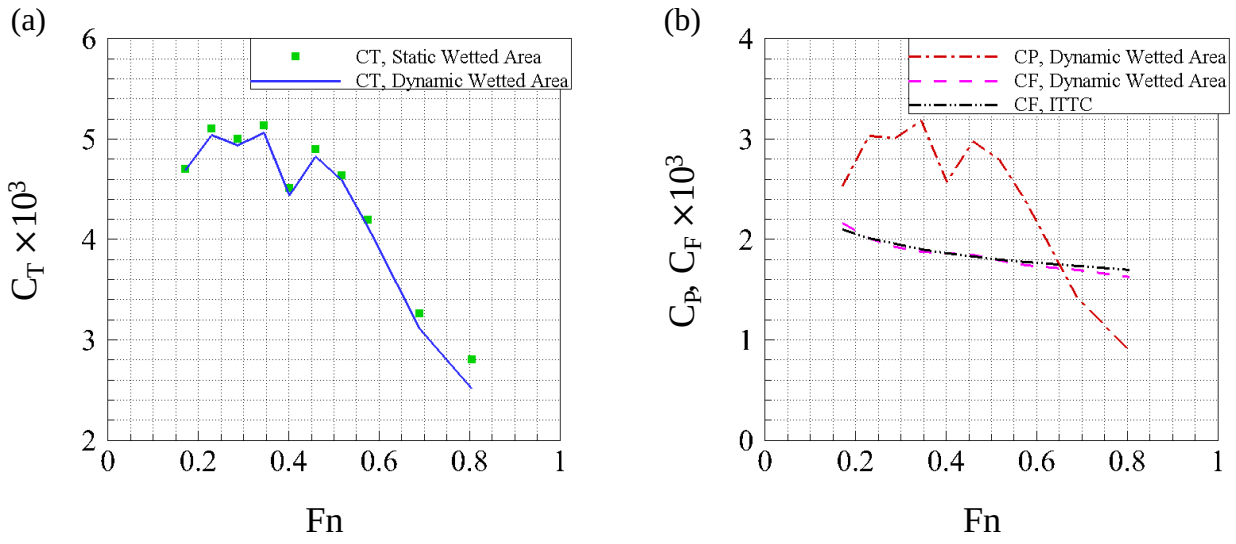

Figure 10 Total resistance coefficient (a), and pressure and frictional resistance coefficients (b) of the London Demonstrator in deep water.

For the shallow water scenario (Figure 11), the resistance coefficient of the catamaran reaches its peak value around the critical depth Froude number and then declines dramatically as the moving speed increases. The maximum C_T value in shallow water is approximately 2.4 times higher than that created in deep water. This ratio is smaller than the value obtained by Castiglione et al. [48] for a similar catamaran configuration, where the C_T peak in shallow water is about 4.2 times larger than that in deep water. Different from the hump of the R_T curve in shallow water, as shown in Figure 9 (a), which is not commonly seen in previous papers, the dramatic increase of C_T near the critical speed has been widely observed in both model tests and numerical simulations [45,48]. It is worth noting that the maximum total resistance coefficient does not correspond to the maxima of the total resistance, according to which the propulsion power should be installed. For the London Demonstrator examined here, the maximum total resistance is accomplished at the highest speed considered here (see Figure 9 (a)), where C_T reaches its minimum value.

Preprints (www.preprints.org) | NOT PEER-REVIEWED | Posted: 26 April 2021 doi:10.20944/preprints202104.0674.v1

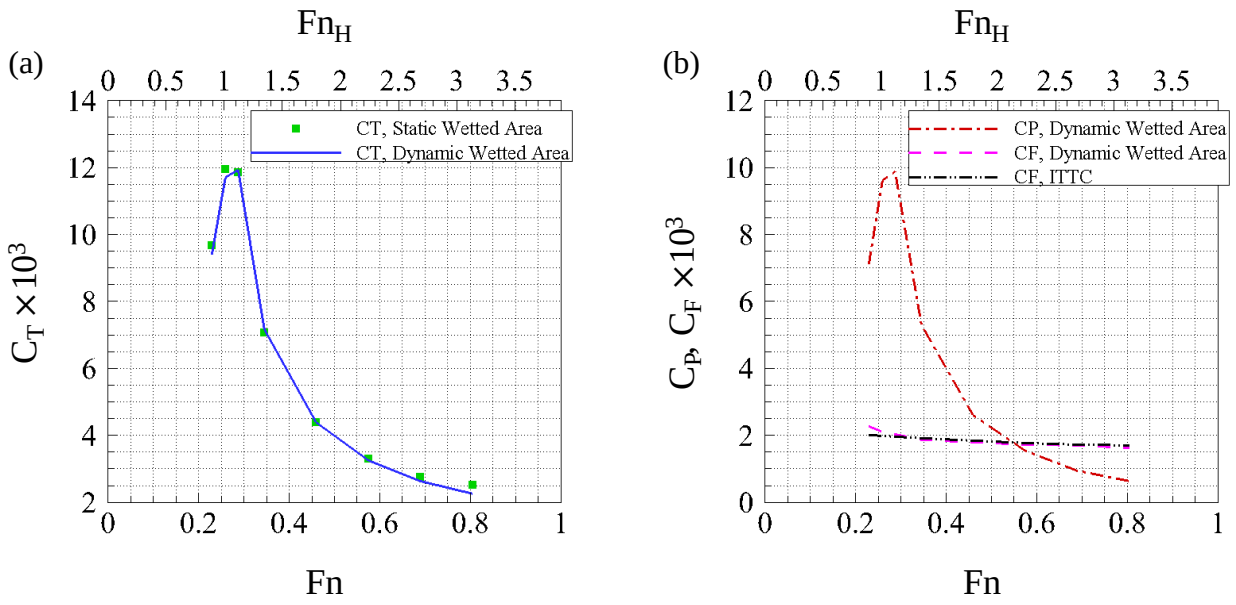

Figure 11 Total resistance coefficient (a), and pressure and frictional resistance coefficients (b) of the London Demonstrator in shallow water (H = 2.15 m).

4.2 Wave patterns

The wave patterns created by the London Demonstrator at various speeds in deep water are demonstrated in Figure 12. The catamaran generates typical Kelvin wave patterns at lower speeds, which comprise of both transverse and divergent waves. As the increase of the Froude number, the amplitude and length of the induced wave also increase while the Kelvin wave angle becomes smaller. Besides, the divergent waves become dominant in the wave pattern at Fn = 0.805. Figure 13 demonstrates the wave elevations of the catamaran in shallow water, which are profoundly different from those shown in Figure 12. As expected, when the depth Froude number is near its critical value (Fn_H = 1.0), the Kelvin wave angle is close to 90 degree and the critical wave is created at Fn_H = 1.12, which is located right in front of the catamaran. The critical wave is normal to the advance direction of the vessel and its attitude is significantly elevated, which leads to the hump observed in the R_T curve in Figure 8 (a) and the remarkable C_T peak shown in Figure 11 (b). Besides, the critical wave significantly elevates the bow, creating the trim maxima observed from Figure 8 (b). Behind the stern of the vessel, divergent waves are generated. As the moving speed increases to the supercritical range, the critical wave disappears and divergent waves are created near both the bow and stern of the hull. The further increase of the Froude number reduces the angles of the divergent waves. However, the overall wave patterns are not significantly changed. In both deep and

Preprints (www.preprints.org) | NOT PEER-REVIEWED | Posted: 26 April 2021 doi:10.20944/preprints202104.0674.v1

shallow water, the decrease of the Kelvin wave angle leads the intersection point of the bow waves created by the two demihulls to move astern, which will be more clearly observed from Figure 14 and Figure 15 as well as the wave cuts demonstrated in the next section.

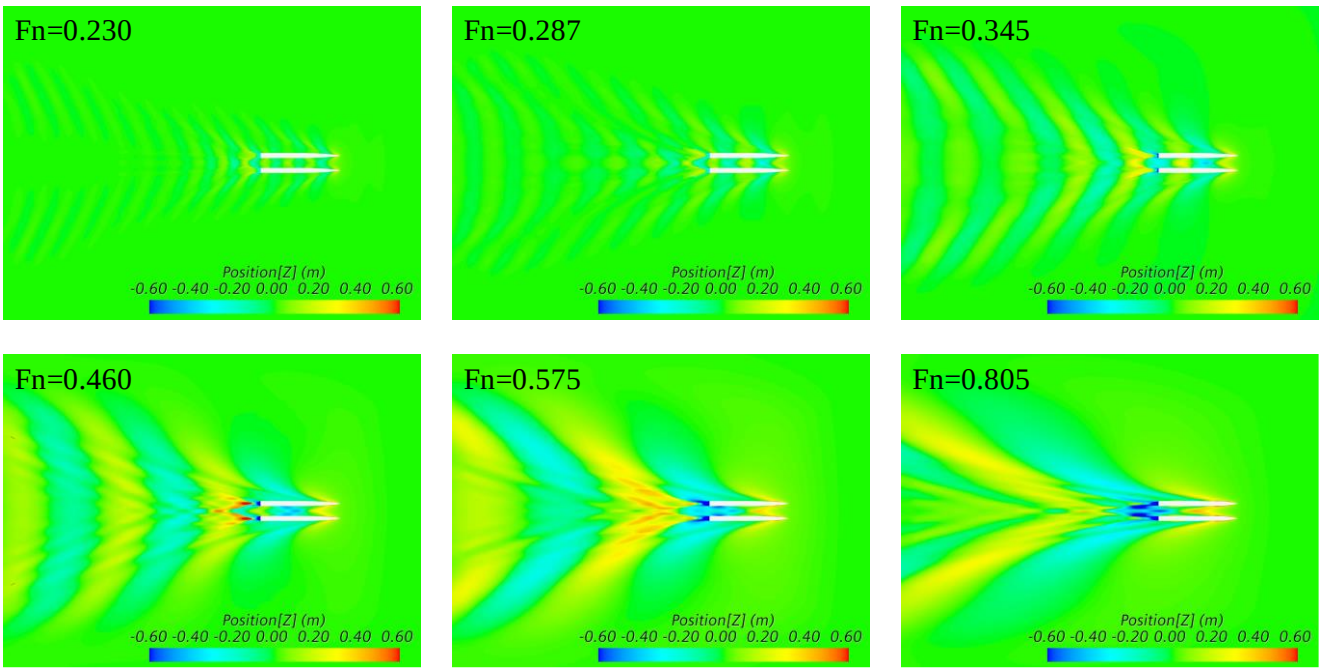

Figure 12 Wave patterns created by the London Demonstrator in deep water.

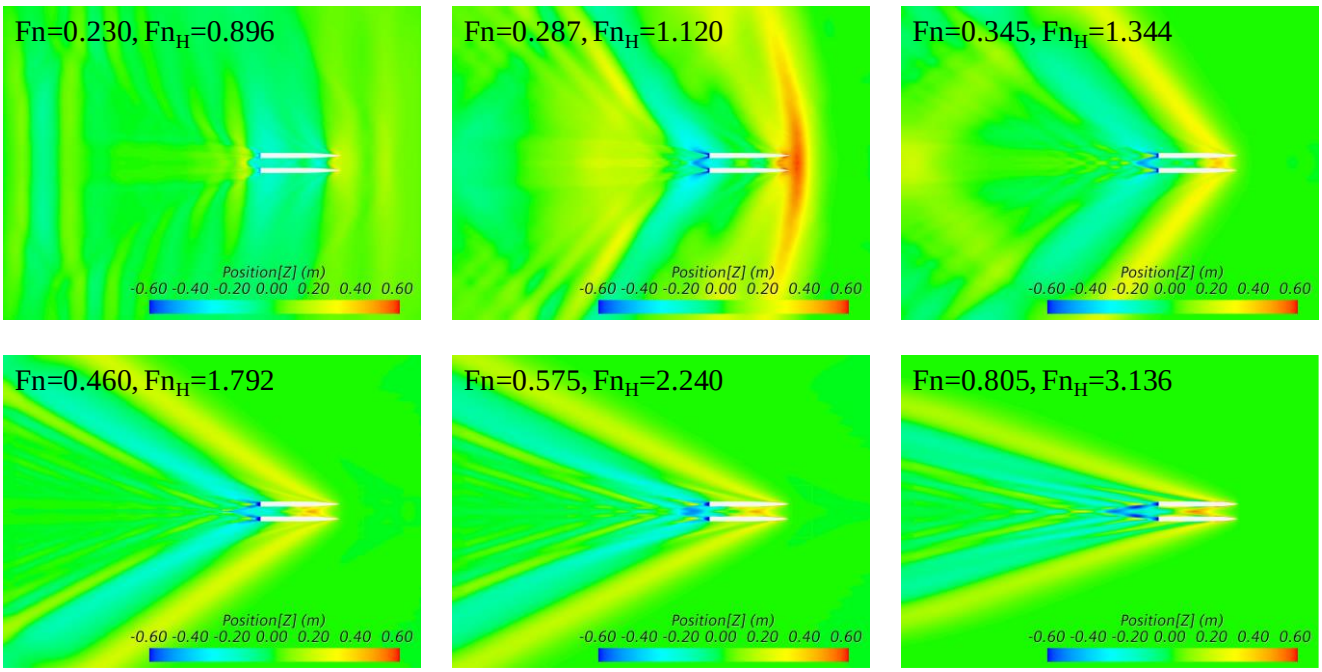

Figure 13 Wave patterns created by the London Demonstrator in shallow water (H = 2.15 m).

Preprints (www.preprints.org) | NOT PEER-REVIEWED | Posted: 26 April 2021 doi:10.20944/preprints202104.0674.v1

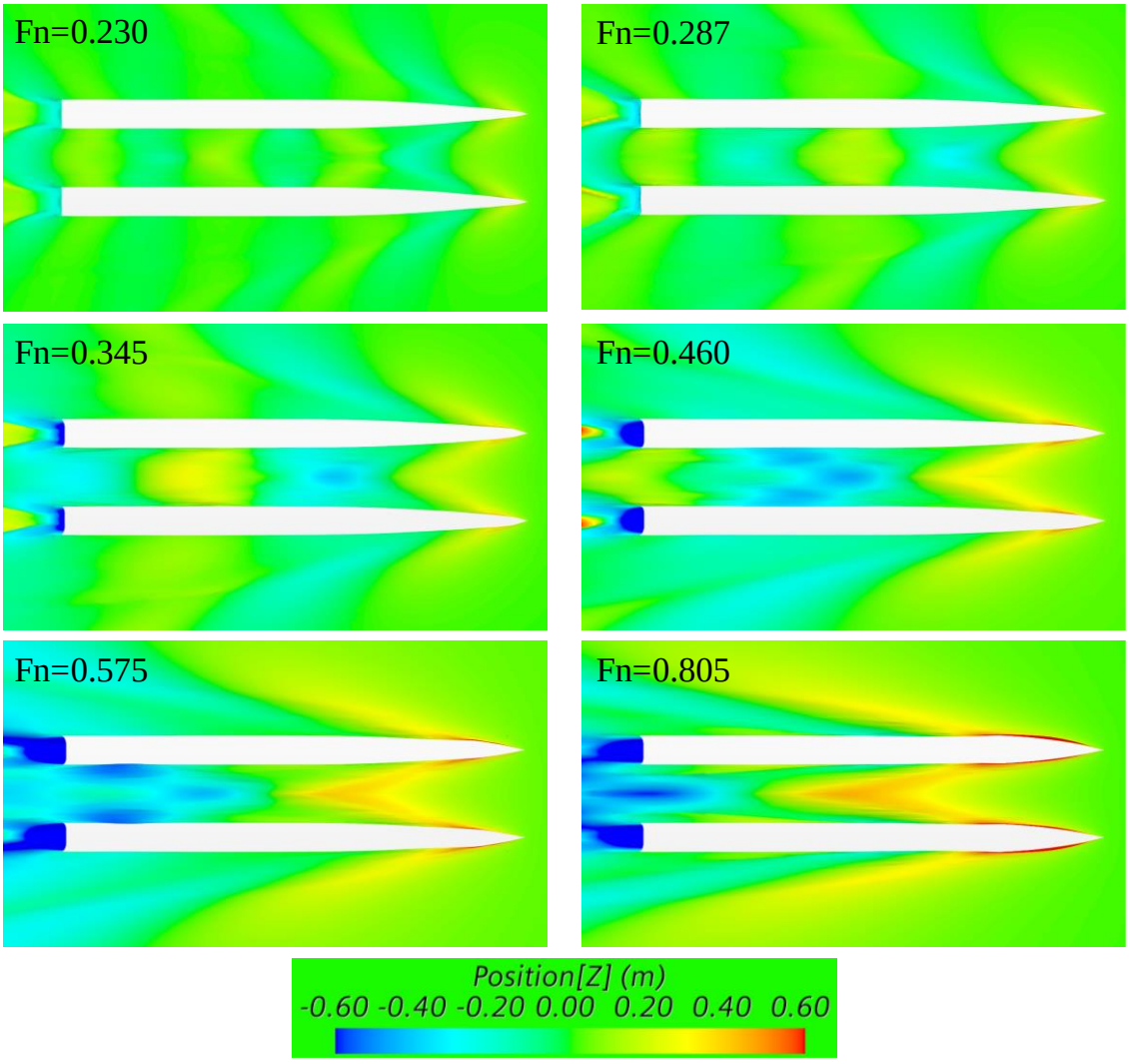

Figure 14 The wave interaction between demihulls in deep water.

The behaviours of the resistance, trim and sinkage discussed in the previous section can be better understood by analysing the interaction between the wave systems generated by the demihulls. Figure 14 shows a closer inspection of the wave interference between the demihulls in deep water. We can observe that at smaller Froude numbers (e.g. when $Fn < 0.3$), multiple crests and troughs exist within the inner region between the two hulls. Enhanced crests and troughs become pronounced when $Fn = 0.345$ at the symmetry plane of the catamaran, where the waves meet and strengthen each other. At $Fn = 0.46$, another two troughs are generated on each side of the symmetry plane apart from the one created at the central plane, indicating a significant secondary wave interference. At this Froude number, the secondary troughs

Preprints (www.preprints.org) | NOT PEER-REVIEWED | Posted: 26 April 2021 doi:10.20944/preprints202104.0674.v1

are located slightly behind midship. As the Froude number increases to 0.575, the crest and troughs between the demihulls are moved further downstream, which has also been reported in previous studies [13,30]. In particular, the secondary wave troughs are generated near the stern with higher amplitudes, which leads to a larger sinkage at the stern, thereby creating the peak of trim as shown in Figure 7 (b). Moreover, as discussed in Figure 9 (a), the pressure resistance R_P reaches its maximum value at Fn = 0.575, implying the wave interference is the strongest at this Froude number. When Fn = 0.805, the wave troughs created due to the secondary wave interaction are moved behind the aft of the catamaran (see Figure 12), which leads to a decrease in the trim as the secondary troughs are closer to the hull surface, thereby having more direct impact on the motion of the demihull. Another observation from the wave pattern at Fn = 0.805 is that the first crest in the inner region is produced near midship, which results in the reduction of the moment causing the pitch motion, leading to the decrease in trim angle. On the other hand, with the first crest further strengthened and moved near the catamaran's centre of mass, this crest will lift the entire catamaran instead of the bow. Therefore, the sinkage becomes negative (the hull moves upward) at higher Froude numbers.

The wave interferences between demihulls in shallow water are demonstrated in Figure 15. Several significant differences from those in deep water can be observed. First, at trans-critical speeds (Fn = 0.23 and 0.287), wave interactions between the demihulls seem to be suppressed due to the creation of the critical wave in front of the catamaran (see Figure 13), i.e., the phenomenon of existing multiple crests and troughs within the inner region disappears. At supercritical speeds (Fn > 0.345), the three troughs observed in deep water (e.g., in Figure 14 when Fn = 0.46) are not seen in shallow water cases. Instead, another two secondary crests are generated apart from the primary one at the catamaran's central plane. As the Froude number increases, the wave crests are stretched and moved towards the stern. As previously discussed, both trim and sinkage will be decreased with the first crest moving midship. This trend will be further enhanced due to the creation of the secondary crests, i.e., at higher speeds, both the trim and sinkage in shallow water are smaller, as seen from Figure 9 (b).

Preprints (www.preprints.org) | NOT PEER-REVIEWED | Posted: 26 April 2021 doi:10.20944/preprints202104.0674.v1

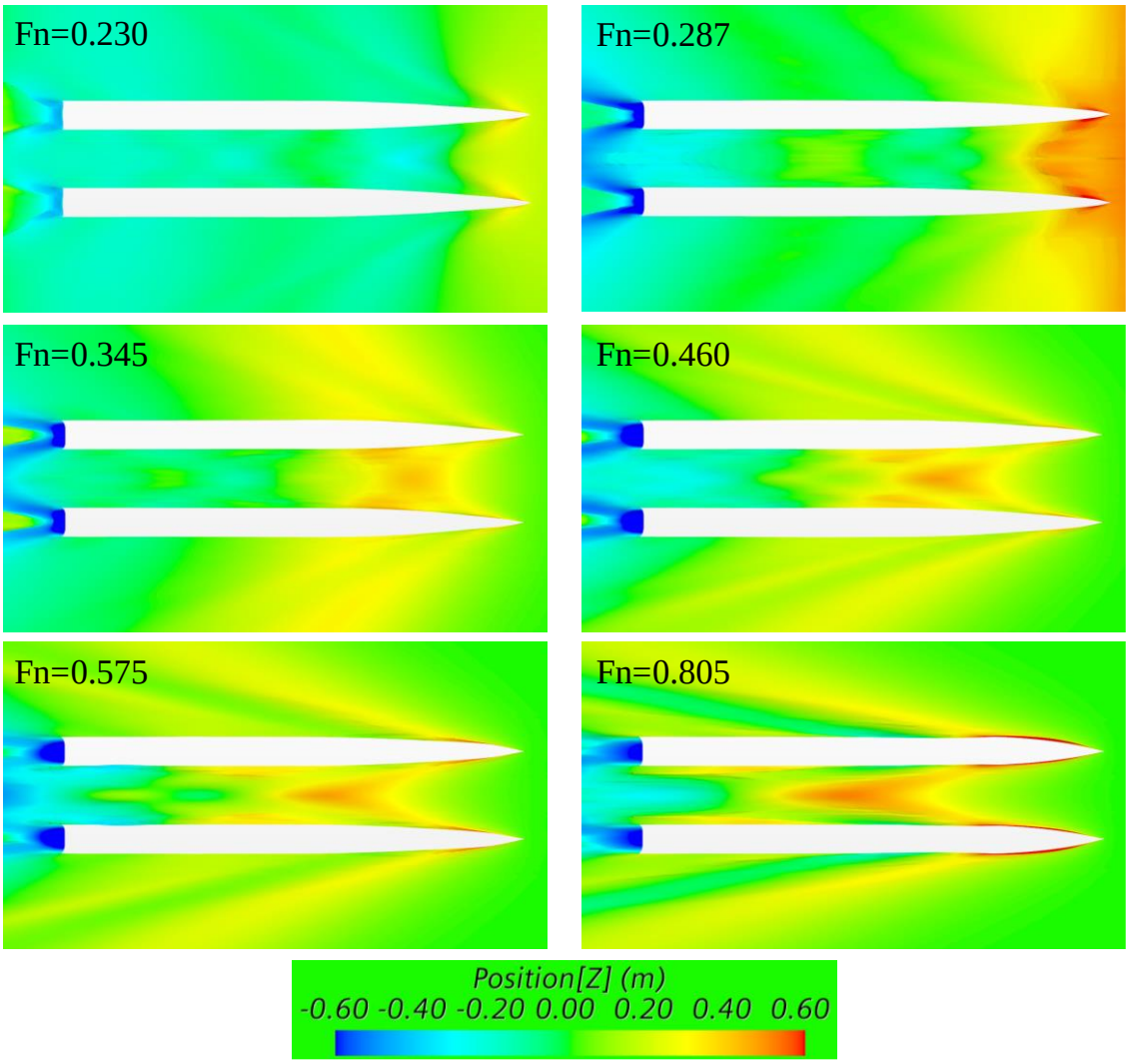

Figure 15 The wave interaction between demihulls in shallow water.

4.3 Longitudinal wave cuts

The wave propagation within the inner region can be better understood by analysing the longitudinal wave cuts at the central plane of the catamaran as demonstrated in Figure 16. It is seen that the wave starts to come into being at the forward perpendicular (FP) for all cases except those at trans-critical speeds (Fn_H = 0.896 and 1.12) in shallow water, where the water is elevated at least $0.5L_{pp}$ ahead of the catamaran and reaches the maximum height near the FP. In deep water, both the wave height and wave length increase as the Froude number rises, confirming the observations from Figure 14. The increase of the wave length leads to a reduction in the number of waves between FP and aft perpendicular (AP). For example, there are approximately three waves between FP and AP when Fn = 0.23 while the number becomes less than

Preprints (www.preprints.org) | NOT PEER-REVIEWED | Posted: 26 April 2021 doi:10.20944/preprints202104.0674.v1

one when Fn increases to 0.805. It is interesting to observe that at Fn = 0.575, the wave number between FP and AP is approximately unity and this Froude number corresponds to the maximum value of the pressure component of total resistance (see Figure 9 (a)). In shallow water, the first wave crest behind the bow is always higher than that created in deep water, especially near the critical speed. The difference is considered small only when the Froude number is greater than 0.575. Moreover, no noteworthy wave troughs are generated between FP and AP in shallow water, which significantly differs from those in deep water. Furthermore, the catamaran generates higher wave crests behind the stern in deep water while creating deeper wave troughs in shallow water.

As observed from previous wave patterns in Figure 14 and Figure 15, the catamaran generates a remarkable trough right behind the stern of the demihull. The magnitude of this trough can be more clearly demonstrated by the longitudinal wave cuts at the mid-plane of the demihull, as shown in Figure 17. In deep water, the magnitude of the trough reaches its maximum value at Fn = 0.575, where the water level difference between FP and AP is also maximised. In shallow water, the trough's magnitudes at trans-critical speeds are significantly larger than those in deep water. The maximum amplitude is achieved at Fn = 0.287, where the critical wave is also created in front of the bow, resulting in a remarkably large difference between the water levels at the FP and AF of the catamaran. It is worth emphasising that Fn = 0.287 and 0.575 correspond to the speeds where the maximum pressure resistance is produced in shallow and deep water respectively, as seen from Figure 9 (a). At supercritical speeds, the trough's amplitude in shallow water becomes smaller than that in deep water, which can be attributed to smaller sinkage and trim created in shallow water.

Preprints (www.preprints.org) | NOT PEER-REVIEWED | Posted: 26 April 2021 doi:10.20944/preprints202104.0674.v1

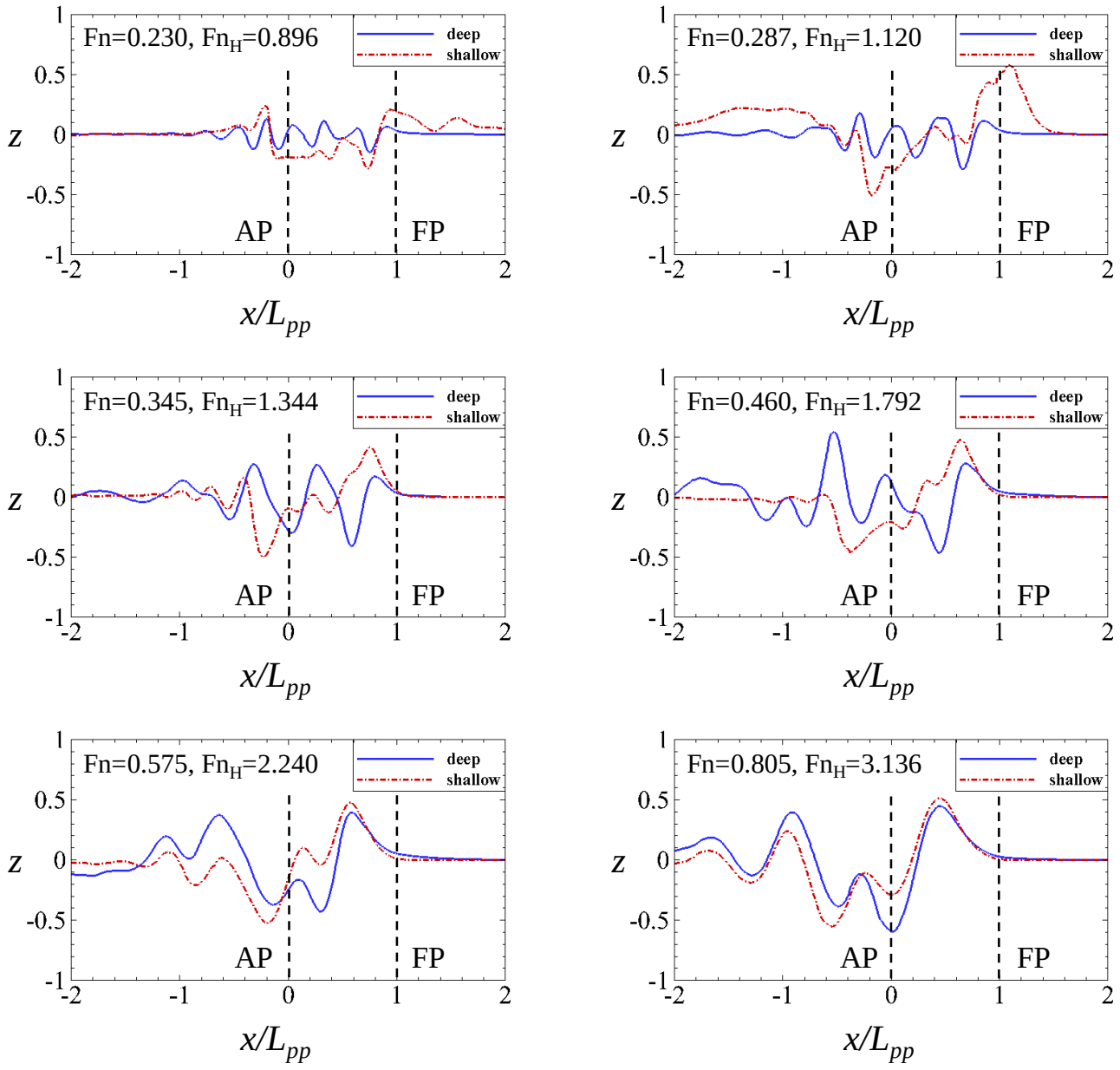

Figure 16 Comparison of the longitudinal wave cuts at the catamaran symmetry plane in deep and shallow water.

Preprints (www.preprints.org) | NOT PEER-REVIEWED | Posted: 26 April 2021 doi:10.20944/preprints202104.0674.v1

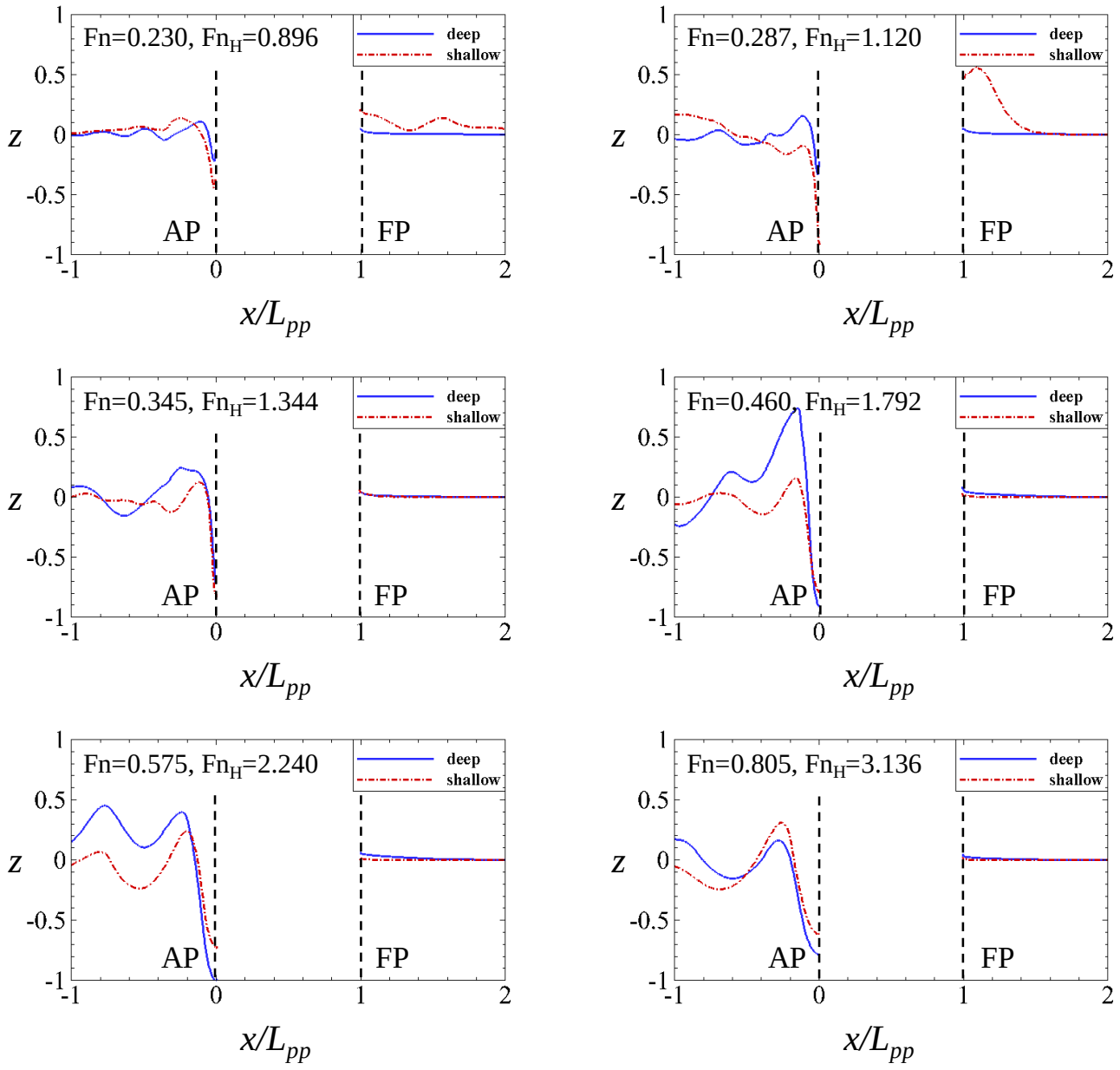

Figure 17 Comparison of the longitudinal wave cuts at the mid-plane of the demihull in deep and shallow water.

Preprints (www.preprints.org) | NOT PEER-REVIEWED | Posted: 26 April 2021 doi:10.20944/preprints202104.0674.v1

4.4 Cross flow fields

With the wave interference between the demihulls, the flow field created by the demihull becomes non-symmetrical against its mid-plane, which will cause a transverse pressure gradient. This can further lead to a cross flow under the keel of the demihull, which is believed to be one of the main causes of the increase in total resistance [31]. The cross flow fields of the London Demonstrator are plotted in Figure 18, where the positive and negative velocities indicate that the flow moves to the outer and inner regions respectively. In deep water, the location and strength of the cross flow are closely associated with the wave interaction between the demihulls. At lower Froude numbers, multiple changes of the cross flow direction under the keel can be observed, which corresponds to the existence of multiple waves between the demihulls (see Figure 14 and Figure 16). With the increase of the Froude number, the strength and extension of the cross flow are significantly enhanced and the locations where the cross flow occurs is also moved towards the stern. This phenomenon was also observed by Zaghi et al. [30] and Farkas et al. [34]. Besides, the number of changes in the cross flow direction is also reduced with the increase of the speed. At higher Froude numbers, significant cross flows are also generated behind the stern. For shallow water scenarios, similar to the deep water cases, the strength of the cross flow is considerably enhanced and the location where the maximum cross flow occurs is also moved towards the stern with the increase of the speed. However, the cross flows created in shallow water are remarkably stronger than the corresponding cases in deep water. Moreover, the phenomenon of multiple changes in cross flow direction observed at lower Froude numbers no longer exists, and for all speeds in shallow water, the cross flow moves from the inner side of the demihull to the outer region.

Preprints (www.preprints.org) | NOT PEER-REVIEWED | Posted: 26 April 2021 doi:10.20944/preprints202104.0674.v1

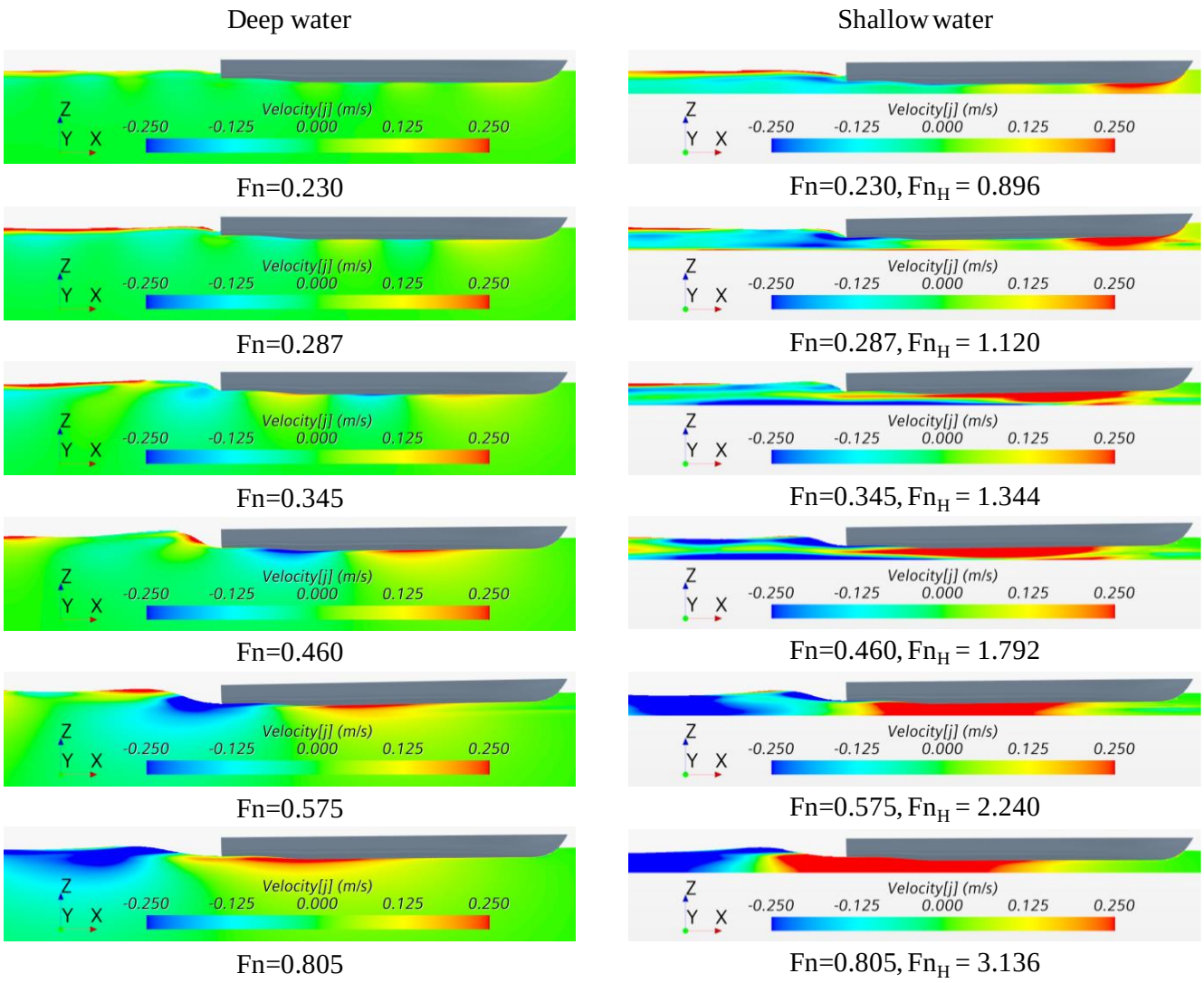

Figure 18 Cross flow fields at the mid-plane of the demihull for deep (left) and shallow (right) water. Positive and negative velocity values mean the flow moves towards the outer and inner sides of the demihull respectively.

5 Conclusion

In the present work, the hydrodynamics of a full scale, zero-emission, high-speed catamaran (London demonstrator) in both deep and shallow water was numerically investigated. The numerical methods used in the current study were validated against experimental data of the NPL 4a02 model [9] and the Stavanger demonstrator [2]. For numerical simulations on the London Demonstrator, a blind validation was also carried out in collaboration with HSVA and good agreement was accomplished.

Preprints (www.preprints.org) | NOT PEER-REVIEWED | Posted: 26 April 2021 doi:10.20944/preprints202104.0674.v1

The resistance, sinkage and trim of the London Demonstrator as functions of Froude number (ranged from 0.2 to 0.8) in deep and shallow water were firstly analysed. The total resistance in deep water increased continuously while in shallow water, a hump was experienced at Fn = 0.287 (Fn_H = 1.12). Besides, the total resistance in shallow water was higher when Fn < 0.45 and became smaller at larger speeds. As the frictional resistance was almost the same in deep and shallow water, i.e., the difference in total resistance was mainly caused by the pressure component. The variations of the pressure resistance were closely related to the behaviours of trim and sinkage. In particular, the maximum trim was accomplished at the Froude number where the pressure resistance was maximised (Fn = 0.287 and 0.575 for shallow and deep water respectively). The largest sinkage in shallow water occurred at the lowest speed whereas in deep water the sinkage reaches its maxima at a Froude number (Fn = 0.517) slightly lower than the one where the maximum trim occurred. Furthermore, the total resistance coefficient curve in deep water showed multiple humps while only one significant peak near the critical speed was produced in shallow water.

The computed wave patterns, longitudinal wave cuts and cross flow fields were also analysed and correlated with the behaviours of the resistance and motion of the catamaran. In general, for both deep and shallow water scenarios, the crests and troughs generated within the inner region were strengthened and moved astern with the increase of Froude number. In deep water, the maximum pressure resistance was related to the creation of a secondary trough near the stern of the demihull. In contrast, the mechanism involved in shallow water was due to the generation of a critical wave in front of the catamaran and normal to the moving direction. Moreover, the creation of maximum pressure resistance was also correlated with the largest water level difference between the forward and aft perpendiculars. Cross flows occurred in both deep and shallow water scenarios due to the asymmetrical flow fields between the inner and outer regions. Compared with deep water cases, the cross flows created in shallow water were much stronger. Moreover, the cross flow in shallow water moved towards the outer region for all speeds considered here, whereas, in deep water, changes in cross flow directions were observed.

Acknowledgement

This work was funded by the H2020 European Union project “TrAM – Transport: Advanced and Modular” (contract 769303). Prof. Boulougouris’ work was partially supported from DNV and Royal Caribbean Group, sponsors of the MSRC. The opinions expressed herein are those of the authors and do not reflect

the views of DNV and Royal Caribbean Group. Results of CFD simulations run by the University of Strathclyde were obtained using ARCHIE-WeSt High Performance Computer (www.archie-west.ac.uk).

Reference

[1] Papanikolaou, A. D. "Review of the Design and Technology Challenges of Zero-Emission, Battery-Driven Fast Marine Vehicles." *Journal of Marine Science and Engineering*, Vol. 8, No. 11, 2020, pp. 1–17. doi:10.3390/jmse8110941.

[2] Papanikolaou, A., Xing-Kaeding, Y., Strobel, J., Kanellopoulou, A., Zaraphonitis, G., and Tolo, E. "Numerical and Experimental Optimization Study on a Fast, Zero Emission Catamaran." *Journal of Marine Science and Engineering*, Vol. 8, No. 9, 2020. doi:10.3390/JMSE8090657.

[3] Mittendorf, M., and Papanikolaou, A. D. "Hydrodynamic Hull Form Optimization of Fast Catamarans Using Surrogate Models." *Ship Technology Research*, Vol. 68, No. 1, 2021, pp. 14–26. doi:10.1080/09377255.2020.1802165.

[4] Wang, H., Boulougouris, E., Theotokatos, G., Priftis, A., Shi, G., Dahle, M., and Tolo, E. "Risk Assessment of a Battery-Powered High-Speed Ferry Using Formal Safety Assessment." *Safety*, Vol. 6, No. 3, 2020. doi:10.3390/safety6030039.

[5] Molland, a. F., Wellicome, J. F., and Couser, P. R. "Theoretical Prediction of the Wave Resistance of Slender Hull Forms in Catamaran Configurations." *Ship Science Report 72, University of Southampton*, 1994.

[6] Shahjada Tarafder, M., and Suzuki, K. "Computation of Wave-Making Resistance of a Catamaran in Deep Water Using a Potential-Based Panel Method." *Ocean Engineering*, Vol. 34, No. 13, 2007, pp. 1892–1900. doi:10.1016/j.oceaneng.2006.06.010.

[7] Bari, G. S., and Matveev, K. I. "Hydrodynamic Modeling of Planing Catamarans with Symmetric Hulls." *Ocean Engineering*, Vol. 115, 2016, pp. 60–66. doi:10.1016/j.oceaneng.2016.01.035.

[8] Insel, M., and Molland, A. F. "An Investigation into the Resistance Components of High Speed Displacement Catamarans." *The Royal Institute of Naval Architects*, Vol. 134, 1992, pp. 1–20.

[9] Molland, A. F., Wellicome, J. F., and Couser, P. R. "Resistance Experiments On A Systematic Series Of High Speed Displacement Catamaran Forms: Variation of Length-Displacement Ratio and Breadth-Draught Ratio." *Ship Science Report 71, University of Southampton*, 1994.

[10] Zaraphonitis, G., Spanos, D., and Papanikolaou, A. "Numerical and Experimental Study on the Wave Resistance of Fast Displacement Asymmetric Catamarans." *Proceedings of International*

Conference on High-Performance Marine Vehicles, Hamburg, Germany., 2001.

[11] van't Veer, R. "Experimental Results of Motions Hydrodynarnic Coefficients and Wave Loads on the 372 Catamaran Model." *Report 1129, Deift University of Technology*, 1998.

[12] Broglia, R., Bouscasse, B., Jacob, B., Olivieri, A., Zaghi, S., and Stern, F. "Calm Water and Seakeeping Investigation for a Fast Catamaran." *11th International Conference on Fast Sea Transportation, FAST 2011 - Proceedings*, 2011, pp. 336–344.

[13] Broglia, R., Jacob, B., Zaghi, S., Stern, F., and Olivieri, A. "Experimental Investigation of Interference Effects for High-Speed Catamarans." *Ocean Engineering*, Vol. 76, 2014, pp. 75–85. doi:10.1016/j.oceaneng.2013.12.003.

[14] Bouscasse, B., Broglia, R., and Stern, F. "Experimental Investigation of a Fast Catamaran in Head Waves." *Ocean Engineering*, Vol. 72, 2013, pp. 318–330. doi:10.1016/j.oceaneng.2013.07.012.

[15] Durante, D., Broglia, R., Diez, M., Olivieri, A., Campana, E. F., and Stern, F. "Accurate Experimental Benchmark Study of a Catamaran in Regular and Irregular Head Waves Including Uncertainty Quantification." *Ocean Engineering*, Vol. 195, No. September 2019, 2020, p. 106685. doi:10.1016/j.oceaneng.2019.106685.

[16] Falchi, M., Felli, M., Grizzi, S., Aloisio, G., Broglia, R., and Stern, F. "SPIV Measurements around the DELFT 372 Catamaran in Steady Drift." *Experiments in Fluids*, Vol. 55, No. 11, 2014. doi:10.1007/s00348-014-1844-z.

[17] Zaraphonitis, G., Papanikolaou, A., and Mourkogiannis, D. "Hull Form Optimization of High Speed Vessels with Respect to Wash and Powering." *Proceedings of 8th International Conference on Marine Design (IMDC), Athens, Greece*, 2003.

[18] Souto-Iglesias, A., Zamora-Rodríguez, R., Fernández-Gutiérrez, D., and Pérez-Rojas, L. "Analysis of the Wave System of a Catamaran for CFD Validation." *Experiments in Fluids*, Vol. 42, No. 2, 2007, pp. 321–332. doi:10.1007/s00348-006-0244-4.

[19] Souto-Iglesias, A., Fernández-Gutiérrez, D., and Pérez-Rojas, L. "Experimental Assessment of Interference Resistance for a Series 60 Catamaran in Free and Fixed Trim-Sinkage Conditions." *Ocean Engineering*, Vol. 53, 2012, pp. 38–47. doi:10.1016/j.oceaneng.2012.06.008.

[20] Danişman, D. B. "Reduction of Demi-Hull Wave Interference Resistance in Fast Displacement Catamarans Utilizing an Optimized Centerbulb Concept." *Ocean Engineering*, Vol. 91, 2014, pp. 227–234. doi:10.1016/j.oceaneng.2014.09.018.

[21] Broglia, R., Zaghi, S., Campana, E. F., Dogan, T., Sadat-Hosseini, H., Stern, F., Queutey, P.,

Visonneau, M., and Milanov, E. “Assessment of Computational Fluid Dynamics Capabilities for the Prediction of Three-Dimensional Separated Flows: The Delft 372 Catamaran in Static Drift Conditions.” *Journal of Fluids Engineering*, Vol. 141, No. 9, 2019, pp. 1–28. doi:10.1115/1.4042752.

[22] Choi, J. E., Min, K. S., Kim, J. H., Lee, S. B., and Seo, H. W. “Resistance and Propulsion Characteristics of Various Commercial Ships Based on CFD Results.” *Ocean Engineering*, Vol. 37, No. 7, 2010, pp. 549–566. doi:10.1016/j.oceaneng.2010.02.007.

[23] Liefvendahl, M., and Fureby, C. “Grid Requirements for LES of Ship Hydrodynamics in Model and Full Scale.” *Ocean Engineering*, Vol. 143, No. March, 2017, pp. 259–268. doi:10.1016/j.oceaneng.2017.07.055.

[24] Romanowski, A., Tezdogan, T., and Turan, O. “Development of a CFD Methodology for the Numerical Simulation of Irregular Sea-States.” *Ocean Engineering*, Vol. 192, No. March, 2019, p. 106530. doi:10.1016/j.oceaneng.2019.106530.

[25] Castiglione, T., Stern, F., Bova, S., and Kandasamy, M. “Numerical Investigation of the Seakeeping Behavior of a Catamaran Advancing in Regular Head Waves.” *Ocean Engineering*, Vol. 38, No. 16, 2011, pp. 1806–1822. doi:10.1016/j.oceaneng.2011.09.003.

[26] He, W., Diez, M., Zou, Z., Campana, E. F., and Stern, F. “URANS Study of Delft Catamaran Total/Added Resistance, Motions and Slamming Loads in Head Sea Including Irregular Wave and Uncertainty Quantification for Variable Regular Wave and Geometry.” *Ocean Engineering*, Vol. 74, 2013, pp. 189–217. doi:10.1016/j.oceaneng.2013.06.020.

[27] Jamaluddin, A., Utama, I. K. A. P., Widodo, B., and Molland, A. F. “Experimental and Numerical Study of the Resistance Component Interactions of Catamarans.” *Journal of Engineering for the Maritime Environment*, Vol. 227, No. 1, 2013, pp. 51–60. doi:10.1177/1475090212451694.

[28] Yengejeh, M. A., Amiri, M. M., Mehdigholi, H., Seif, M. S., and Yaakob, O. “Numerical Study on Interference Effects and Wetted Area Pattern of Asymmetric Planing Catamarans.” *Journal of Engineering for the Maritime Environment*, Vol. 230, No. 2, 2016, pp. 417–433. doi:10.1177/1475090215586638.

[29] Zha, R. S., Ye, H. X., Shen, Z. R., and Wan, D. C. “Numerical Computations of Resistance of High Speed Catamaran in Calm Water.” *Journal of Hydrodynamics*, Vol. 26, No. 6, 2015, pp. 930–938. doi:10.1016/S1001-6058(14)60102-5.

[30] Zaghi, S., Broglia, R., and Di Mascio, A. “Analysis of the Interference Effects for High-Speed

Catamarans by Model Tests and Numerical Simulations." *Ocean Engineering*, Vol. 38, No. 17–18, 2011, pp. 2110–2122. doi:10.1016/j.oceaneng.2011.09.037.

[31] Broglia, R., Zaghi, S., and Di Mascio, A. "Numerical Simulation of Interference Effects for a High-Speed Catamaran." *Journal of Marine Science and Technology*, Vol. 16, No. 3, 2011, pp. 254–269. doi:10.1007/s00773-011-0132-3.

[32] He, W., Castiglione, T., Kandasamy, M., and Stern, F. "Numerical Analysis of the Interference Effects on Resistance, Sinkage and Trim of a Fast Catamaran." *Journal of Marine Science and Technology*, Vol. 20, No. 2, 2015, pp. 292–308. doi:10.1007/s00773-014-0283-0.

[33] Haase, M., Zurcher, K., Davidson, G., Binns, J. R., Thomas, G., and Bose, N. "Novel CFD-Based Full-Scale Resistance Prediction for Large Medium-Speed Catamarans." *Ocean Engineering*, Vol. 111, 2016, pp. 198–208. doi:10.1016/j.oceaneng.2015.10.018.

[34] Farkas, A., Degiuli, N., and Martić, I. "Numerical Investigation into the Interaction of Resistance Components for a Series 60 Catamaran." *Ocean Engineering*, Vol. 146, No. May, 2017, pp. 151–169. doi:10.1016/j.oceaneng.2017.09.043.

[35] Ferreiro, L. D. "The Effects of Confined Water Operations on Ship Performance." *Naval Engineers Journal*, 1992, pp. 69–83.

[36] Jachowski, J. "Assessment of Ship Squat in Shallow Water Using CFD." *Archives of Civil and Mechanical Engineering*, Vol. 8, No. 1, 2008, pp. 27–36. doi:10.1016/s1644-9665(12)60264-7.

[37] Tezdogan, T., Incecik, A., and Turan, O. "A Numerical Investigation of the Squat and Resistance of Ships Advancing through a Canal Using CFD." *Journal of Marine Science and Technology*, Vol. 21, No. 1, 2016, pp. 86–101. doi:10.1007/s00773-015-0334-1.

[38] Terziev, M., Tezdogan, T., Oguz, E., Gourlay, T., Demirel, Y. K., and Incecik, A. "Numerical Investigation of the Behaviour and Performance of Ships Advancing through Restricted Shallow Waters." *Journal of Fluids and Structures*, Vol. 76, 2018, pp. 185–215. doi:10.1016/j.jfluidstructs.2017.10.003.

[39] Feng, D., Ye, B., Zhang, Z., and Wang, X. "Numerical Simulation of the Ship Resistance of KCS in Different Water Depths for Model-Scale and Full-Scale." *Journal of Marine Science and Engineering*, Vol. 8, No. 10, 2020, pp. 1–25. doi:10.3390/jmse8100745.

[40] Chen, X. N., Sharma, S. D., and Stuntz, N. "Wave Reduction by S-Catamaran at Supercritical Speeds." *Journal of Ship Research*, Vol. 47, No. 2, 2003, pp. 145–154. doi:10.5957/jsr.2003.47.2.145.

[41] Castiglione, T., He, W., Stern, F., and Bova, S. "Effects of Shallow Water on Catamaran Interference." *11th International Conference on Fast Sea Transportation, FAST 2011*, 2011, pp. 371–376.

[42] Moraes, H. B., Vasconcellos, J. M., and Latorre, R. G. "Wave Resistance for High-Speed Catamarans." *Ocean Engineering*, Vol. 31, No. 17–18, 2004, pp. 2253–2282. doi:10.1016/j.oceaneng.2004.03.012.

[43] Zhu, Y., Ma, C., Wu, H., He, J., Zhang, C., Li, W., and Noblesse, F. "Farfield Waves Created by a Catamaran in Shallow Water." *European Journal of Mechanics, B/Fluids*, Vol. 59, 2016, pp. 197–204. doi:10.1016/j.euromechflu.2016.06.003.

[44] Molland, A. F., Wilson, P. A., and Taunton, D. J. "A Systematic Series of Experimental Wash Wave Measurements for High Speed Displacement Monohull and Catamaran Forms in Shallow Water." *Ship Science Report 122, University of Southampton*, 2001. doi:10.3940/rina.ijme.2004.a2.3604.

[45] Molland, A. F., Wilson, P. A., and Taunton., D. J. "Resistance Experiments on a Systematic Series of High Speed Displacement Monohull and Catamaran Forms in Shallow Water." *Ship Science Report 127, University of Southampton*, 2003.

[46] Gourlay, T. "Sinkage and Trim of a Fast Displacement Catamaran in Shallow Water." *Journal of Ship Research*, Vol. 52, No. 3, 2008, pp. 175–183. doi:10.5957/jsr.2008.52.3.175.

[47] Lee, S. H., Lee, Y. G., and Kim, S. H. "On the Development of a Small Catamaran Boat." *Ocean Engineering*, Vol. 34, No. 14–15, 2007, pp. 2061–2073. doi:10.1016/j.oceaneng.2007.02.011.

[48] Castiglione, T., He, W., Stern, F., and Bova, S. "URANS Simulations of Catamaran Interference in Shallow Water." *Journal of Marine Science and Technology*, Vol. 19, No. 1, 2014, pp. 33–51. doi:10.1007/s00773-013-0230-5.

[49] Gatchell, S., Hafermann, D., and Streckwall, H. "Open Water Test Propeller Performance and Cavitation Behaviour Using PPB and FreSCo+." *Proceedings in the Second International Symposium on Marine Propulsors, Hamburg, Germany*, 2011.